KERNFORSCHUNGSANLAGE JÜLICH

des Landes Nordrhein-Westfalen

Energy Dependence of Deuteron Scattering by Magnesium

von

C. Mayer-Böricke, R. Santo
und U. Schmidt - Rohr

Jül - 30 - KP

November 1961

Als Manuskript gedruckt

Max-Planck-Institut für Kernphysik, Heidelberg

Berichte der Kernforschungsanlage Jülich – Nr. 30

Dok.: DEUTERONS - SCATTERING * DK 539.128.2.172

Zu beziehen durch: ZENTRALBIBLIOTHEK der Kernforschungsanlage Jülich,
Jülich, Bundesrepublik Deutschland

Energy Dependence of Deuteron Scattering by Magnesium

von

C. Mayer-Böricke, R. Santo
und U. Schmidt - Rohr

ENERGY DEPENDENCE OF DEUTERON SCATTERING BY MAGNESIUM

C. Mayer-Böricke, R. Santo and U. Schmidt-Rohr.

Max-Planck-Institute for Nuclear Physics, Heidelberg, Germany

(To be published in part in NUCLEAR PHYSICS)

Abstract

The angular distributions of elastic and inelastic (Q = -1.37 MeV) deuteron scattering from Mg have been measured at 8.65, 9.97, 10.87 and 11.80 MeV in 5^{o} -steps. These results as well as those from other authors have been discussed in terms of a diffraction scattering model. In the range of deuteron-energies from 8 - 22 MeV the interaction radii deduced from elastic data decrease slightly with increasing energy. The interaction radii from the analysis of the inelastic scattering data do not agree in all cases studied with the corresponding radii from elastic data. The deformation parameter for Mg^{24} was found to be $|\beta_2| = 0.22$.

Tables of all inelastic 11.8 MeV deuteron scattering data obtained in our laboratory are presented in the appendix.

I. INTRODUCTION

Angular distributions of medium energy deuterons scattered elastically or inelastically by light nuclei, such as Mg, show typically a diffraction-like pattern with well-defined, regular minima and maxima. Patterns of similar kind with sharp and persistent oscillations are well known too from the scattering of α-particles. The "diffraction scattering model with strong absorption"[1] was used with considerable success in alalyzing such angular distributions, especially for α-particles[1-3]. Within certain limitations it gives a consistent interpretation for both elastic and inelastic scattering processes in cases where the inelastic process excites a low-lying level of a collective nature. If a ratational level is excited, as in Mg^{24}, only two free parameters enter the description: the interaction radius, R_o, and the deformation parameter, β_2. R_o should normally have the same value irrespective of whether it is taken from the analysis of elastic or inelastic experimental data. One of the results of an extensive analysis in terms of this model [3] was that in α-scattering by Mg the interaction radius from fits to elastic and inelastic data was really the same and that this radius was independent of energy. Contrary to this result we found from a preliminary analysis of 11.8 MeV deuteron scattering data [4] that the interaction radii from independent best fits to elastic and inelastic scattering by Mg were not the same. On the other hand Blair et al. [3] found equality of these radii in an anlalysis of their 21 MeV d-scattering data. Therefore the present work was undertaken to study more extensively the energy dependence of the interaction radii for d-scattering.

The nucleus Mg^{24}, for which some measurements [3-12] are already available, is well suited for such an investigation. The experimental reason favoring Mg as a target is the large spacing of the levels, so that the deuterons scattered from the 1.37 MeV level may be easily separated from the elastic deuteron group and from the inelastic groups due to excitation of higher levels.

Particularly extensive investigations in scattering by Mg were done for protons [13].

II. EXPERIMENTAL

The angular distributions of the scattered deuterons were measured with a 20 cm diameter scattering chamber, the apparatus and experimental method being identical with those described in ref. [4] The primary beam energy of 11.8. MeV was reduced to 10.87, 9.97 and 8.65 MeV by placing aluminum absorbers in front of the collimator system at the entrance to the scattering chamber. The incident beam energy was determined by measuring the deuteron-range in aluminum. For that purpose foils of various thicknesses were rotated into the beam. From these range measurements we obtained the mean energies using the range-energy-relations of Bichsel, Mozley and Aron [15]. Due to the resolution of the Cs I-counter the half-width of the elastic peak in our spectra was normally about 4 % at 11.8 MeV. It was broadened by the aluminum absorbers up to 7.5 % at 8.65 MeV. The targets used had thicknesses of 2.7 and 4.1 mg/cm^2 and were rolled from commercial foils with a purity better than 99 %. For every energy absolute scattering cross sections were determined at a laboratory

angle of 50^{o}. For these measurements a Faraday cup was used with a current integrator in connection with a calibrated, highly-sensitive galvanometer. Besides this the absolute cross section of gold was measured in the same arrangement and geometry for comparison. It was always found to be in good agreement with previous careful measurements.[16] Our elastic scattering cross sections refer to the natural isotopic mixture and the inelastic cross sections to Mg^{24}. The errors in the determination of the absolute cross sections are approximately $\pm$ 10 %. They arise from inhomogeneity of the targets, the statistical errors and the background in the spectra. The statistical errors change with angle from $\pm$ 3 % at forward angles up to $\pm$ 6 % at backward angles. The error in the determination of the inelastic cross section is mainly due to the uncertainly in unfolding the elastic and inelastic peaks from each other and from the background in the spectrum. These errors are estimated to be at most $\pm$ 5 %.

III. RESULTS

Fig. 1 shows a typical spectrum of deuterons scattered by Mg, obtained from a pulse height analyzer at an angle of 90^{o} and 11.8 MeV beam energy. The results for elastic and inelastic scattering are shown in fig. 2 and fig. 3 respectively, the elastic results being presented as the ratio of the observed to the Rutherford cross section. Both types of distributions have the shape of an interference pattern with pronounced maxima, which shift with decreasing energy towards larger angles. From fig. 2 one can see that the interference structure is washed out for angles larger than $\sim 120^{o}$. In

most cases no pronounced additional maximum is observed in this region. Matsudo et al.[13] found a vanishing of the structure in the angular distributions for proton scattering on Mg between 8 and 9 MeV. A similar effect was not seen in our deuteron scattering data.

Some very measurements are available for comparison with our work. The results of Hinds and Middleton [17] at 10 MeV are in good agreement with our elastic 9.97 MeV curve. Another elastic measurement of Freindl et al.[18] at 13 MeV fits well into the set of angular distributions presented in fig. 2.

IV. ANALYSIS AND DISCUSSION

IV. a. General

It is known that Mg^{24} is a deformed even-even nucleus with 0^+-groundstate and a first excited collective 2^+-state of rotational character at 1.37 MeV [19)20)]. The diffraction scattering model, which is based on collective excitation, should therefore be appropriate for scattering by Mg^{24}. Indeed it was used successfully in explaining the main features of α-scattering angular distributions of this nucleus over a wide range of energies[3]. Also some deuteron data were analyzed in terms of this model [1)3)9)].

The treatment of the scattering problem within the framework of this theory is very similar to that of classical Fraunhofer diffraction of light by a little black ellipsoid. Really one goes beyond this classical analogy only in that one includes in the description the quantum mechanical properties of the collective states of the target nucleus involved in the

scattering process. This is easily done in an adiabatic approximation. In this way the model is able to predict the elastic cross section as well as the inelastic scattering amplitudes exciting discrete collective rotational states. The theory neglects the Coulomb field of the nucleus and is not valid for scattering at larger angles. The model has been used in the analysis of the present deuteron scattering experiments. For an even-even nucleus the elastic scattering cross section in the centre-of-mass system is given in simple approximate form by [1)3)]

$$(1a) \qquad d\sigma/\Omega = (kR_o^2)^2 \left[J_1(x)/x\right]^2$$

or with inclusion of the slowly varying "obliquity factor" $\cos^2 \Theta/2$ [2)] by

$$(1b) \qquad d\sigma/d\Omega = \cos^2 \Theta/2 \, (kR_o^2)^2 \left[J_1(x)/x\right]^2 ,$$

where $x = 2kR_o \sin O/2$. For inelastic scattering with excitation of the first 2^+-rotational-level one obtains a similar expression [1)3)] consistent with (1a)

$$(2) \qquad d\sigma/d\Omega = (kR_o^2)^2 \beta_2^2/4 \left[J_o^2(x)/4 - 3J_2^2(x)/4\right]$$

The obliquity factor again may be introduced as in (1b). Θ is the scattering angle and k the wave number of the incident deuteron in the c.m. system. The J_1 are ordinary Besselfunctions, β_2 is the quadrupole deformation parameter and R_o is the interaction radius. R_o and β_2 are only free parameters. They were determined by fitting the theoretical expressions. (1a),

(1b) and (2) to the experimental angular distributions in the range of angles less than about 120^{o}. These calculations were mainly done on a Siemens 2002 digital compuer[+].

IV. b. Elastic scattering

In this case R_o is the only free parameter. It is determined by the locations of the experimental maxima. The obliquity factor in (1b) does not appreciably change the locations of the initial theoretical maxima in (1a) so that R_o is the same in both cases, but the overall fit according to (1b) was always somewhat better than that according to (1a). In fig. 4 our elastic data and the measurements of ref.[4] and ref.[11] are shown together with the theoretical curves. The 21.6 MeV measurement is similar to the measurements of Greenlees and Lowe [10] at 19.6. MeV and of Blair Farwell and McDaniels [3] at 21 MeV. The overall agreement between experiment and theory is good, especially for the lower energy data in figs. 4a - 4d. The characteristic shape of the angular distribution in its main features is reproduced by theory over several orders of magnitude. With the exception of fig. 4e the absolute cross sections are predicted quite accurately in the forward directions, particularly in the vicinity of the first maximum. One can see from fig. 4 that the second maximum drops progressively below the theoretical prediction as the energy is increased from 8.65 to 11.8 MeV. At considerab-

---

[+]Thanks are due to Dr. Krüger and Dr. Rothleitner of the Institute for Theoretical Physics of the University of Heidelberg for help in programming the calculations for the machine.

ly higher energies as in fig. 4e even the first experimental maximum falls below the curves calculated from eqs. 1a and 1b. At higher orders of the diffraction pattern this difference increases. This difficulty is similar to that known from α-particle scattering analysis and is inherent in the model [1-3] †).

- It is interesting to note that the interaction radius R_o is not exactly the same for the five different energies in fig. 4. To study the energy dependence of R_o in more detail we have analyzed all measurements known to us from other laboratories. The resulting R_o -values in the energy range from 7-23 MeV are given in fig. 5. The radii corresponding to the best fits to the angular distributions are marked by thick bars. The range of possible radii is indicated at each energy. It is mainly due to experimental uncertainties. Fig. 5 shows that R_o is only constant to a first approximation (mean value 6.4 f) and that there is a tendency for slowly decreasing radii as one proceeds to higher energies. At the end of the energy range considered (21.6 MeV) R_o lies between 6.0 and 6.25 f with the best fit at 6.16 f. This coincides with the findings of Blair et al. [3] in analyzing the 22.8 MeV elastic α-particle scattering data of Hu et al [21], which give a best fit at R_o = 6.02 f. From the energy depen-

---

†) A contribution to this question was given quite recently by J. Berysowiez and J. Dabrowski, Proc. Ruth. Jub. Conf. Manch. (1961) C 2/50

dence of R_o in fig. 5 it may be supposed that in the higher energy region considered in α-scattering analysis [3] the interaction radii from deuteron scattering and α-scattering are essentially the same. Blair et al. found the α-interaction radii to be very constant with a mean value of 5.97 f over the α-energy range from 20-50 MeV. The slowly decreasing R_o-values may be associated with the loose structure of the deuteron and possibly with effects due to the nuclear Coulomb-field.

As may be seen from (1b) and (1a), the model predicts [3] that the angular distributions may always be reduced to the same single universal curve (which is independent of energy and kind of the incident, strongly absorbed particle) if one plots the diffrential cross section after division by a simple term as a function of the scattering argument $x = 2kR_o \sin \theta/2$. Since in our case R_o depends somewhat on energy we divided $d\sigma/d\Omega$ according to (1b) by the term $(k R_o^2 \cos \theta/2)^2$. The factor $\cos^2 \theta/2$, which improves somewhat the fit beyond the initial maximum in the ordinate-direction, may be omitted without changing the conclusions to be drawn in the following discussion. The results are given in fig. 6 for the measurements with the Heidelberg-cyclotron up to 11.8 MeV and for three more measurements between 19.6 and 21.6 MeV.

The group of angular distributions at lower energies ($\leq$ 11.8 MeV) fits the theoretical curve quite well and displays a universal behavior up to $x \cong 7$. It is only in the region of the second maximum that the data differ considerably from each other. Here the height of the maximum drops

gradually with increasing energy in the sense of the general energy dependence in fig. 6, which is displayed clearly if one compares the groups of measurements around 10 and 20 MeV with each other. These two groups at essentially different energies show up in the diagram as well separated patterns of similar shape. At about 20 MeV the reduced cross sections fall considerably below the theoretical curve and the data of the 10 MeV group. At the second and third maximum this effect is even more pronounced than at the initial one. The universality prediction is displayed only with respect to the correspondence between the locations of minima and maxima of the two patterns but is not realized with respect to the amplitudes. There may be several reasons for the breakdown of the universality prediction. The structure of the deuteron and the relatively large d-wavelengths may play a role. It therefore seems possible that the universal behavior of the reduced data may be better displayed in a higher energy region, where it has already been shown to exist for α-particles. At small x-values the shape of the reduced patterns changes somewhat. The first minimum becomes deeper and the first maximum more pronounced if the energy is increased. This effect may possibly be understood [3] in terms of the nuclear Coulomb field, which gradually loses importance as one increases the d-energy.

IV. c. Inelastic scattering

Fig. 7a shows our measurements at 8.65 MeV compared with theory. Both parameters, R_o and β_2, were varied in the calculations. The agreement between the theoretical curve according to (2) and the experimental data is very satisfactory.

It is typical for all our measurements and is displayed rather well even at larger angles, especially at 9.97 MeV (fig. 7b). If one proceeds from the energy region around 10 MeV to higher energies the experimental curve gradually becomes steeper as in the elastic patterns. If the theoretical curve is normalized by the value of the parameter β_2 to the first experimental maximum, the higher order experimental maxima soon drop with increasing energy below the theoretical curves, whether or not one includes the obliquity factor. This behavior is demonstrated in fig. 8, where the reduced experimental data of Hinds et al. [6], Jahr et al. [4] up to 120° and Blair et al. [3] are included for comparison. As in the diagram of the reduced elastic data the locations of minima and maxima agree quite well for the different curves but the peak heights of the maxima fall more and more below the theoretical curve as one increases the energy. For our data at low energies there is again (as in the case of elastic data) good agreement with theory, especially in the region below 120°. The R_o-and β_2-values given in fig. 8 are those from the best possible fits to the inelastic experimental angular distributions, irrespective of the elastic R_o-values.
For a more complete study of R_o as a function of energy we have again analyzed all available data. The result is presented in fig. 5b. Because of well-known experimental difficulties, the inelastic data are sometimes more scanty than the elastic ones. Thus, for instance, the R_o-values of the preliminary inelastic 15.9 and 17.5 MeV data and those of 19.6 MeV are rather uncertain. As can be seen immediately from fig. 6b the values of the interaction radius scatter much more about

the mean value of 6.2 f than in fig. 5a. The R_o -values between 9.5 and 12 MeV are considerably smaller than the corresponding elastic interaction radii. This is in contrast to the findings of Blair et al.[3] for α-particles, where it was always possible to fit the inelastic data with the R_o -value extracted from the corresponding elastic distribution. It is mainly in the upper part (>15 MeV) of the d-energy range considered that elastic and inelastic radii are equal at each energy, i.e., the ranges of possible R_o -values in fig. 5a and 5b overlap. It would be interesting therefore to see whether in the region of α-energies considered by Blair et al. (≈22 MeV) this regular behavior of R_o is also displayed in d-scattering data. The β_2 -values from the analysis of the inelastic scattering data are given in table 1. They correspond to a normalization of the theoretical curve to the experiments at the first maximum. The mean value of about 0.22 agrees well with the corresponding $|\beta_2|$ from α-scattering[3] (0.24).

V. CONCLUSIONS

The following conclusions may be drawn from the analysis of the elastic and inelastic deuteron scattering data.

1) At low energies one can fit the experimental angular distributions well by the diffraction scattering formulas (1a), (1b) and (2) (fig. 4a-c, fig. 7). At higher energies both the elastic and inelastic experimental angular distributions show the same characteristic behavior: with increasing energy they fall progressively below the theoretical predictions (fig. 6 and fig. 8).

2) The interaction radii deduced from the analysis of elastic

deuteron data decrease slightly with energy (fig. 5a) and are at 22 MeV approximately equal to the radii from elastic α-particle scattering analysis.

3) For $E_d \gtrsim 15$ MeV the interaction radii from the inelastic deuteron data agree with the radii from the corresponding elastic distributions. At some lower energies they seem to be different from the elastic radii.

ACKNOWLEDGEMENTS

The authors wish to thank Professor W. Gentner for his support and interest. Thanks are due to Mr. S. Martin for assistance in the calculations.

References

1) J. S. Blair, Phys. Rev. 115 (1959) 928
E. V. Inopin, J. Exptl. Theoret. Phys. (U.S.S.R.) 31 (1956) 901 (Soviet. Phys. JETP 4 (1957) 764)
S. I. Drozdov, J. Exptl. Theoret. Phys. (U.S!S.R.) 28 (1955) 734, 736 (Soviet. Phys. JETP 1 (1955) 588, 591)

2) D.K. McDaniels, J. S. Blair, S. W. Chen and G. W. Farwell, Nuclear Physics 17 (1960) 614

3) J. S. Blair, G.W. Farwell and D. K. McDaniels, Nuclear Physics 17 (1960) 641

4) R. Jahr, K. D. Müller, W. Oswald and U. Schmidt-Rohr, Z. Physik 161 (1961) 5o9

5) J. R. Holt and C. T. Young, Nature 164 (1949) 1000

6) S. Hinds, R. Middleton and G. Parry, Proc. Phys. Soc. A70 (1957) 900

7) O. F. Nemets and G. A. Prokopets, Soviet. Phys. JETP 11 (1960) 499

8) J. W. Haffner, Phys. Rev. 103 (1956) 1398

9) A.G. Blair and E. W. Hamburger, Phys. Rev. 122 (1961) 566

10) G.W. Greenlees and J. Lowe, Proc. Phys. Soc. A76 (1960) 149

11) J. L. Yntema, Phys. Rev. 113 (1958) 261

12) Private communications of the Osaka-cycloton group concerning preliminary data on 15.9 and 17.5 MeV elastic and on 11.15, 15.9 and 17.5 MeV inelastic scattering by Mg.

13) K. Matsudo, Y. Nagahara, Y. Oda, N. Yamamuro and S. Kobayashi, Nuclear Physics 27 (1961) 1

14) A. Doehring, R. Jahr and U. Schmidt-Rohr, Z. Physik 159 (1960) 149

15) H. Bichsel, R. F. Mozley and W. A. Aron, Phys. Rev. 105 (1958) 1788

16) G. Igo, W. Lorenz and U. Schmidt-Rohr, Phys. Rev. (to be published)

17) S. Hinds and R. Middleton, Proc. Ruth, Jub. Conf. Manch. (1961) C5/50

18) L. Freindl, H. Niewodniczanski, J. Nurzynski, M. Slapa and A. Strzalkowski, Proc. Ruth. Jub. Conf. Manch. (1961) C5/21

19) G. Rakavy, Nuclear Physics 4 (1957) 375

20) A. E. Litherland, H. McManus, E.B. Paul, D.A. Bromley and H. E. Gove, Can. J. Phys. 36 (1958) 378

21) Hu, Kato, Oda and Takeda, Journ. Phys. Soc. (Japan) 14 (1959) 539

APPENDIX

E_d MeV	$\|\beta_2\|$	ref.
8.65	0.23	+)
8.9	0.23	6)
9.97	0.21	+)
10.87	0.25	+)
11.8	0.25	4)
14.8	0.20	9)
15.1	0.22	8)
17.5	0.18	12)
21	0.22	3)

+) present work

Table 1. Parameters $|\beta_2|$ as determined from the analysis of inelastic d-scattering angular distributions of Mg^{24}.

Scattering cross sections for Magnesium at 8.65 MeV

Mg (d,d) Q = 0		$Mg^{24}(d,d')Mg^{24*}$ Q=-1.37 MeV	
Θ_{cm}	σ_{cm}[mbarn/sterad]	Θ_{cm}	σ_{cm}[mbarn/sterad]
27.0	$7.00 \cdot 10^{2}$		
32.4	2.78	32.6	$7.47 \cdot 10^{0}$
37.7	1.18	38.0	9.64
43.0	$6.86 \cdot 10^{1}$	43.3	7.04
48.4	5.77	48.7	4.60
53.6	5.14	54.0	2.10
58.9	3.96	59.3	1.79
64.1	2.58	64.5	2.78
69.3	1.52	69.7	3.20
74.5	$7.99 \cdot 10^{0}$	74.9	4.14
79.6	4.93	80.1	3.98
84.7	4.26	85.2	3.53
89.7	4.70	90.2	3.37
94.8	5.24	95.2	2.51
99.7	5.06	100.2	1.94
104.7	4.33	105.2	1.56
109.6	3.43	110.1	1.55
114.5	2.40	114.9	1.46
119.3	1.94		
[degree]		[degree]	

Scattering cross sections for Magnesium at 9.97 MeV

Mg (d,d) Q = 0		$Mg^{24}(d,d')\ Mg^{24*}$ Q = -1.37 MeV	
θ_{cm}	σ_{cm} [mbarn/sterad]	θ_{cm}	σ_{cm} [mbarn/sterad]
21.6	$1.27 \cdot 10^{3}$		
26.5	$5.62 \cdot 10^{2}$		
31.9	$2.16 \cdot$	32.1	$6.64 \cdot 10^{0}$
37.2	$8.95 \cdot 10^{1}$	37.4	6.67
42.5	5.12	42.8	3.61
47.9	5.12	48.1	2.06
53.1	4.66	53.4	1.47
58.4	3.32	59.2	1.73
64.6	1.72	65.0	2.13
69.8	$9.86 \cdot 10^{0}$	70.2	2.82
74.5	5.33	74.9	3.68
80.4	3.36	80.5	3.49
84.7	3.93	85.1	3.23
89.7	3.96	90.2	2.52
94.8	3.93	95.2	1.92
99.7	3.42	100.7	1.51
104.2	2.64	104.6	1.35
110.1	2.04	110.5	1.39
114.5	1.81	114.9	1.59
119.3	1.43	119.7	1.69
124.1	1.30	125.0	1.97
128.9	1.27	128.7	2.13
133.6	1.06	133.9	2.03
138.4	$9.50 \cdot 10^{-1}$	138.1	2.21
143.0	9.10	143.8	2.32
147.7	8.60	147.4	2.16
151.9	7.60	152.6	2.16
157.0	8.20	156.7	1.92
161.6	8.90	162.2	2.04
166.2	$1.02 \cdot 10^{0}$	165.8	1.82
[degree]		[degree]	

Scattering cross sections for Magnesium at 10.87 MeV

Mg (d,d) Q = 0		$Mg^{24}(d,d')MG^{24*}$ Q =-1.37 MeV	
Θ_{CM}	σ_{CM}[mbarn/sterad]	Θ_{CM}	σ_{CM}[mbarn/sterad]
22.1	$1.14 \cdot 10^{3}$		
27.0	$3.77 \cdot 10^{2}$	27.1	$5.94 \cdot 10^{0}$
32.4	$1.47 \cdot 10^{2}$	32.5	$1.10 \cdot 10^{1}$
37.7	$6.20 \cdot 10^{1}$	37.9	$8.20 \cdot 10^{0}$
43.0	5.09 .	43.3	5.38
48.4	5.52	48.6	2.35
53.6	4.46	53.9	1.59
58.9	2.91	59.2	1.97
64.1	1.44	64.4	2.67
69.3	$7.40 \cdot 10^{0}$	69.6	4.10
74.5	4.05	74.8	4.55
79.6	4.12	80.0	4.05
85.2	4.60	85.1	3.23
89.7	5.21	90.1	2.51
94.8	4.63	95.1	1.82
99.7	3.58	100.1	1.35
104.2	2.58	105.1	1.21
109.6	2.01	110.0	1.14
114.5	1.63	114.8	1.28
119.3	1.27	119.6	1.52
124.1	1.10	124.4	1.91
128.9	$9.73 \cdot 10^{-1}$	129.2	2.07
133.6	8.22	133.9	2.35
138.4	7.63	138.6	2.21
143.0	7.04	143.3	2.26
147.7	6.62	147.9	2.24
152.4	6.23	152.5	2.12
157.0	6.15	157.1	1.74
161.6	6.30	161.7	1.83
166.2	7.10	166.3	1.80
[degree]		[degree]	

Scattering cross sections for Magnesium at 11.8 MeV

Mg(d,d) Q = 0		Mg(d,d') Q=-1.37 MeV [+)]		Mg(d,d') Q= -4.12 MeV -4.24 MeV	
Θ_{CM} [degree]	σ_{CM} [mbarn/ster]	Θ_{CM} [degree]	σ_{CM} [mbarn/ster]	Θ_{CM}	σ_{CM} [mbarn/ster]
21.7	$1.12 \cdot 10^{3}$				
23.8	$8.54 \cdot 10^{2}$	24.5	7.16		
24.9	6.38				
27.1	4.04	28.3	8.06		
29.2	2.29				
30.3	1.87				
32.5	1.17	32.6	8.33	33.1	2.42
37.8	$4.89 \cdot 10$	37.9	7.23	38.5	2.51
43.2	5.18	43.3	4.60	44.0	2.12
48.5	5.67	48.6	2.65	49.4	1.80
53.8	4.09	53.9	1.93	54.7	1.45
59.1	2.15	59.2	2.02	60.1	1.38
64.3	$9.02 \cdot 10^{0}$	64.4	2.31	65.4	1.18
69.4	4.17	69.6	2.73	70.7	1.25
74.6	3.44	74.8	2.77	75.7	1.16
79.7	4.11	80.0	2.47	80.9	1.27
84.8	4.25	85.0	2.06	86.1	1.23
89.8	3.62	90.1	1.71	91.1	1.22
94.8	2.71	95.1	1.50	96.1	1.27
99.8	1.95	100.0	1.45	101.1	1.24
104.8	1.38	105.0	1.27	106.0	1.19
109.7	1.08	109.8	1.29	110.8	1.17
114.6	1.03	114.7	1.29	115.7	1.03
119.3	1.03	119.5	1.40	120.5	1.01
124.1	1.01	124.3	1.37	125.3	$9.32 \cdot 10^{-1}$
128.8	$9.30 \cdot 10^{-1}$	129.1	1.45		
133.6	8.61	133.8	1.61		
138.3	7.10	138.5	1.57		
143.0	6.21	143.2	1.64		

continued....

Θ_{CM} [degree]	σ_{CM} [mbarn/ster.]	Θ_{CM} [degree]	continued σ_{CM} [mbarn/ster.]
147.7	$5.93 \cdot 10^{-1}$	147.9	1.55
152.4	5.79	152.6	1.44
157.o	5.39	157.2	1.31
161.6	5.5o	161.8	1.19
166.2	6.15	166.4	1.1o

+) The isotopic abundance of Mg^{24} is not taken into account in the case of Mg(d,d'), Q = -1.37 MeV.

Scattering cross sections for Carbon at 11.8 MeV

Θ_{cM} [degree]	C(d,d), Q = 0 σ_{cM} [mbarn/ster]	Θ_{cM} [degree]	C(d,d') Q = -4,43 MeV σ_{cM} [mbarn/ster]
25	$3.53 \cdot 10^{2}$	24	12.0
30	1.63		
35	$5.41 \cdot 10^{1}$	28	9.3
40	$8.26 \cdot 10^{0}$	36.5	8.2
42.5	5.05	42.5	7.2
45	9.18		
50	$2.57 \cdot 10^{1}$	48.5	6.6
55	3.35	54.o	6.o
6o	3.o3	6o.o	5.5
65	2.2o	65.5	5.7
7o	1.42		
75	$8.72 \cdot 1o^{0}$	71.o	5.7
8o	4.82	77.o	6.3
85	2.75	82.5	6.9
9o	1.93		
95	1.54	88.o	6.8
100	1.42	93.o	6.6
1o5	1.47		
11o	1.61	98.o	5.o
115	2.18	[degree]	
12o	3.o7		
125	3.76		
13o	4.59		
135	5.o5		
14o	5.19		
145	5.41		
15o	5.64		
155	6.33		
16o	7.34		
165	9.32		
[degree]			

Scattering cross sections for Titan at 11.8 MeV

Θ_{CM} [degree]	Ti (d,d), Q = 0 σ_{CM} [mbarn/ster.]	Ti (d,d'), Q = -0,99 MeV σ_{CM} [mbarn/ster.]
31.2	4.03 . 10^2	3.28 . 10^0
36.4	1.75	2.56
41.5	1.35	1.87
46.7	1.oo	1.93
51.8	7.16 . 10^1	1.92
57.o	3.89	1.71
62.1	2.10	1.28
67.2	1.40	9.18 . 10^{-1}
72.3	9.29 . 10^0	7.25
77.3	7.8o	8.1o
82.4	6.7o	8.36
87.4	6.13	8.31
92.4	5.59	7.o9
97.4	4.98	6.12
1o2.4	3.87	4.53
1o7.4	2.91	4.17
112.3	1.79	3.98
117.2	1.24	4.68
122.1	1.o5	4.64
127.o	1.18	4.74
131.9	1.33	4.23
136.7	1.51	4.o6
141.6	1.5o	3.79
146.4	1.42	3.52
151.2	1.2o	3.52
156.o	9.3o . $1o^{-1}$	3.66
16o.8	7.o5	3.84
165.6	5.37	4.o9

Scattering cross sections for Iron at 11.8 MeV

Θ_{CM} [degree]	Fe (d,d), Q = 0 σ_{CM}[mbarn/ster.]	Fe (d,d'), Q = - 0.845 MeV σ_{CM}[mbarn/ster.]
41.3	$2.24 \cdot 10^{2}$	3.00
46.5	1.35	1.87
51.6	$8.46 \cdot 10$	1.79
56.7	3.96	1.32
61.8	2.27	1.12
66.9	1.65	1.10
72.0	1.51	1.11
77.0	1.31	1.08
82.0	1.07	$9.47 \cdot 10^{-1}$
87.0	$7.32 \cdot 10^{0}$	7.32
92.0	5.40	5.40
97.0	3.96	4.05
102.0	2.88	3.19
107.0	2.26	3.15
112.0	1.96	3.33
116.9	1.78	3.50
121.8	1.69	3.57
126.7	1.59	3.34
131.6	1.50	2.94
136.5	1.32	2.38
141.3	1.15	2.08
146.2	$8.87 \cdot 10^{-1}$	1.93
151.1	7.85	1.84
155.9	7.14	1.79
160.7	6.84	1.89
165.6	6.96	1.80

Scattering cross sections for Nickel at 11.8 MeV

θ_{cm} [degree]	Ni (d,d), Q = 0 σ_{cm} [mbarn/ster.]	Ni (d,d'), Q=-(1.42±0.10) MeV σ_{cm} [mbarn/ster.]
31.0	$7.52 \cdot 10^{2}$	4.27
36.1	3.64	3.03
41.3	2.47	2.37
46.4	1.64	1.72
51.5	$8.78 \cdot 10^{1}$	1.36
56.6	4.44	1.12
61.7	2.69	$9.86 \cdot 10^{-1}$
66.8	2.31	9.89
71.9	2.15	9.60
76.9	1.74	9.26
82.0	1.32	9.38
87.0	$9.00 \cdot 10^{0}$	8.15
92.0	5.97	5.56
97.0	4.32	3.88
102.0	3.34	2.94
106.9	3.07	2.82
111.9	3.02	2.91
116.9	2.87	3.18
121.8	2.59	3.73
126.7	2.17	3.80
131.6	1.71	3.10
136.5	1.34	2.70
141.3	1.10	2.21
146.2	$9.91 \cdot 10^{-1}$	1.87
151.0	9.69	1.57
155.9	$1.00 \cdot 10^{0}$	1.46
160.7	1.11	1.46
165.5	1.24	1.56

Scattering cross sections for Copper at 11.8 MeV

Θ_{CM} [degree]	Cu (d,d), Q = 0	Cu (d,d') Q = $-\begin{cases} 0,96 \pm 0,10 \\ 1.27 \pm 0.10 \end{cases}$ MeV
	σ_{CM} [mbarn/ster.]	σ_{CM} [mbarn/ster.]
36.1	$4.38 \cdot 10^{2}$	3.26
41.2	2.77	2.08
46.3	1.50	1.23
51.4	$7.83 \cdot 10$	1.08
56.5	4.14	$9.63 \cdot 10^{-1}$
61.6	3.20	7.92
66.7	2.72	7.51
71.8	2.38	6.93
76.8	1.79	6.54
81.8	1.17	6.37
86.8	$6.82 \cdot 10^{0}$	4.48
91.8	4,83	2.85
96.8	4.20	2.00
101.8	4.12	1.84
106.8	3.95	2.06
111.7	3.63	2.53
116.7	2.92	2.77
121.6	2.32	2.66
126.5	1.92	2.19
131.4	1.46	1.66
136.3	1.19	1.27
141.2	1.15	$9.03 \cdot 10^{-2}$
146.1	1.09	8.38
150.9	1.07	8.75
155.8	1.12	9.33
160.6	1.12	$1.05 \cdot 10^{-1}$
165.5	1.11	1.16

Scattering cross sections for Zinc at 11.8 MeV

Θ_{CM} [degree]	Zn (d,d), Q = 0	Zn (d,d'), Q = -(o,96±o,1o)MeV
	σ_{CM} [mbarn/ster.]	σ_{CM} [mbarn/ster.]
30.9	1.03 . 10^3	4.6o
36.o	4.62 . $1o^2$	3.56
41.2	2.8o	2.35
46.3	1.76	2.11
51.4	9.22 . 1o	1.9
56.4	5.4o	1.9
61.5	4.14	1.9
66.6	3.58	1.72
71.7	2.73	1.67
76.7	1.91	1.29
81.7	1.28	8.86 . $1o^{-1}$
86.8	8.o4 . 10^o	7.16
91.8	6.o7	4.58
96.7	4.92	4.23
1o1.7	4.6o	4.12
1o6.7	4.22	4.82
111.7	3.35	4.99
116.6	2.8o	4.31
121.5	2.2o	3.93
126.5	1.84	3.39
131.4	1.51	2.66
136.3	1.28	1.85
141.2	1.22	1.68
146.o	1.13	1.74
15o.9	1.22	1.95
155.8	1.13	2.12
16o.6	1.11	2.17
165.5	9.97 . $1o^{-1}$	2.59

Figure Captions

Fig. 1. A typical pulse height spectrum of deuterons scattered by Mg. (1) Elastic line, (2) Q = -1.37 MeV (Mg^{24}), (3) Q = -4.12 MeV and Q = -4.24 MeV (Mg^{24}).

Fig. 2. Ratio of the elastic d-scattering cross sections from Mg to the Rutherford cross sections as a function of Θ_{cm}. (The 11.8 MeV data, which coincide with our own measurements, were taken from ref. [4])

Fig. 3. Differential cross sections of deuterons inelastically scattered from the 1.37 MeV level of Mg^{24} as a function of Θ_{cm}. (Again the 11.8 MeV data were taken from ref. [4]).

Fig. 4. Comparison between experimental angular distributions and theoretical curves accroding to (1b) for elastic d-scattering from Mg. In fig. 4d the dashed line represents formula (1a). The experimental curves in figs. 4d and e are taken from ref. [4] and [11].

Fig. 5. Energy dependence of the interaction radius R_o for (a) elastic and (b) inelastic deuteron scattering by Mg and Mg^{24*} (1.37 MeV), respectively, as determined independently from fits to the elastic and inelastic experimental data using eqs. (1a), (1b) and (2).

Fig. 6. Comparison between reduced elastic angular distributions for several energies. For 19.6, 21.0 and 21.6 MeV the data of ref. [10], [3] and [11] were used, respectively. The solid line gives the theoretical prediction of the diffraction scattering model

according to (1b). The presentation of data is confined to x-values corresponding to $\Theta < 120^{\circ}$. The diagram without inclusion of the obliquity factor $\cos^2\Theta/2$ looks very similar. Only the fit to the theoretical curve in the ordinate-direction, particularly at the second and third maximum is somewhat inferior.

Fig. 7. Experimental angular distributions of inelastic d-scattering (Mg^{24} (d, d') Mg^{24*} (1.37 MeV) at 8.65 and 9.97 MeV compared with theory (eq. (2)). The dashed line in fig. 7a gives the theoretical fit with inclusion of the term $\cos^2\Theta/2$ and $|\beta_2| = 0.25$ for comparison.

Fig. 8. Comparison between the reduced experimental inelastic scattering distributions for several energies. For 8.9, 11.8 and 21 MeV the measurements of ref. [6], [4] and [3] were used, respectively. The solid line gives the theoretical prediction of the diffraction scattering model according to (2).

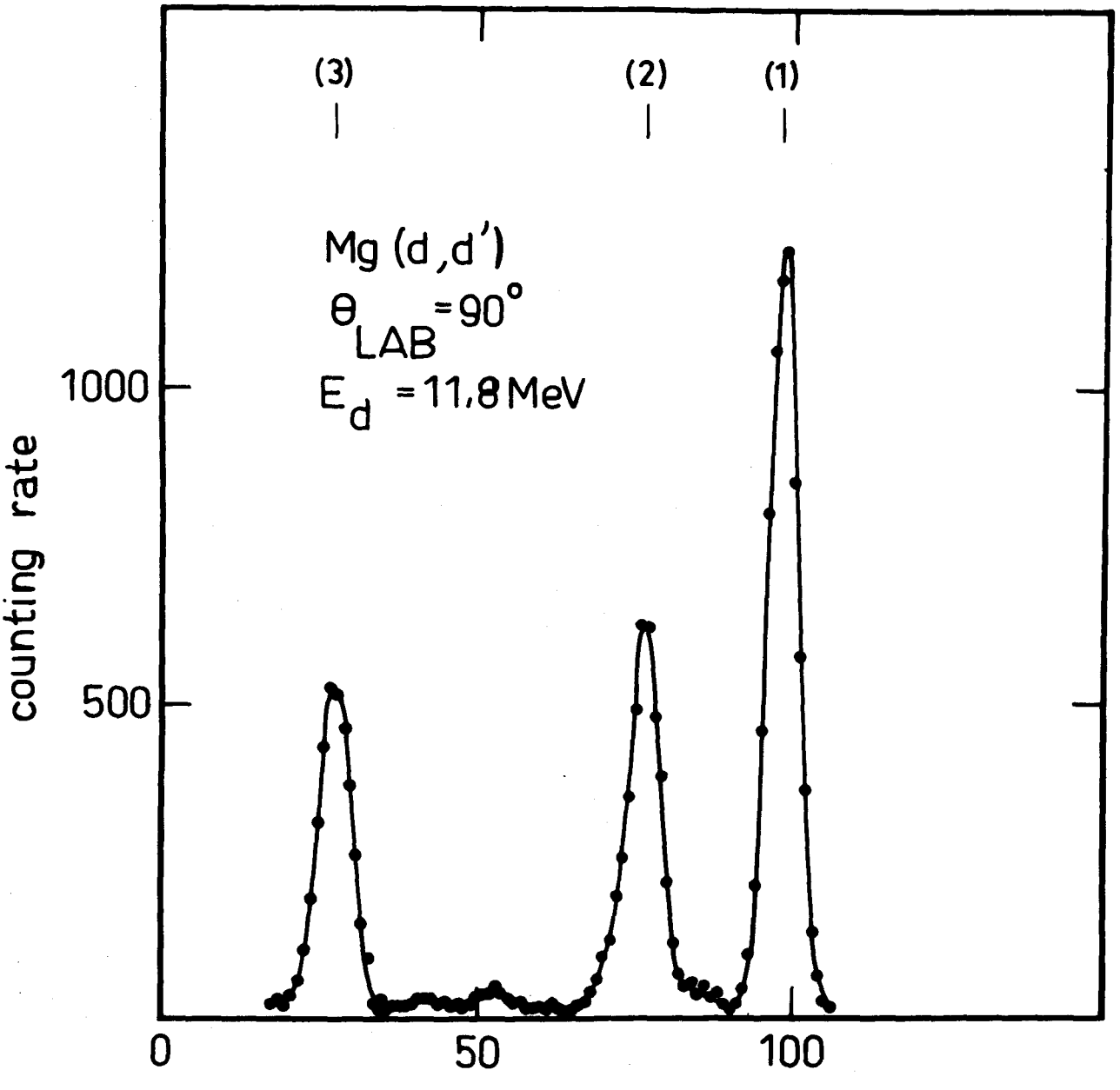
(3)
(2)
(1)
Mg (d,d')
θ LAB = 90°
E d = 11,8 MeV
1000
500
counting rate
0
50
100
channel number (pulse height)

fig. 1

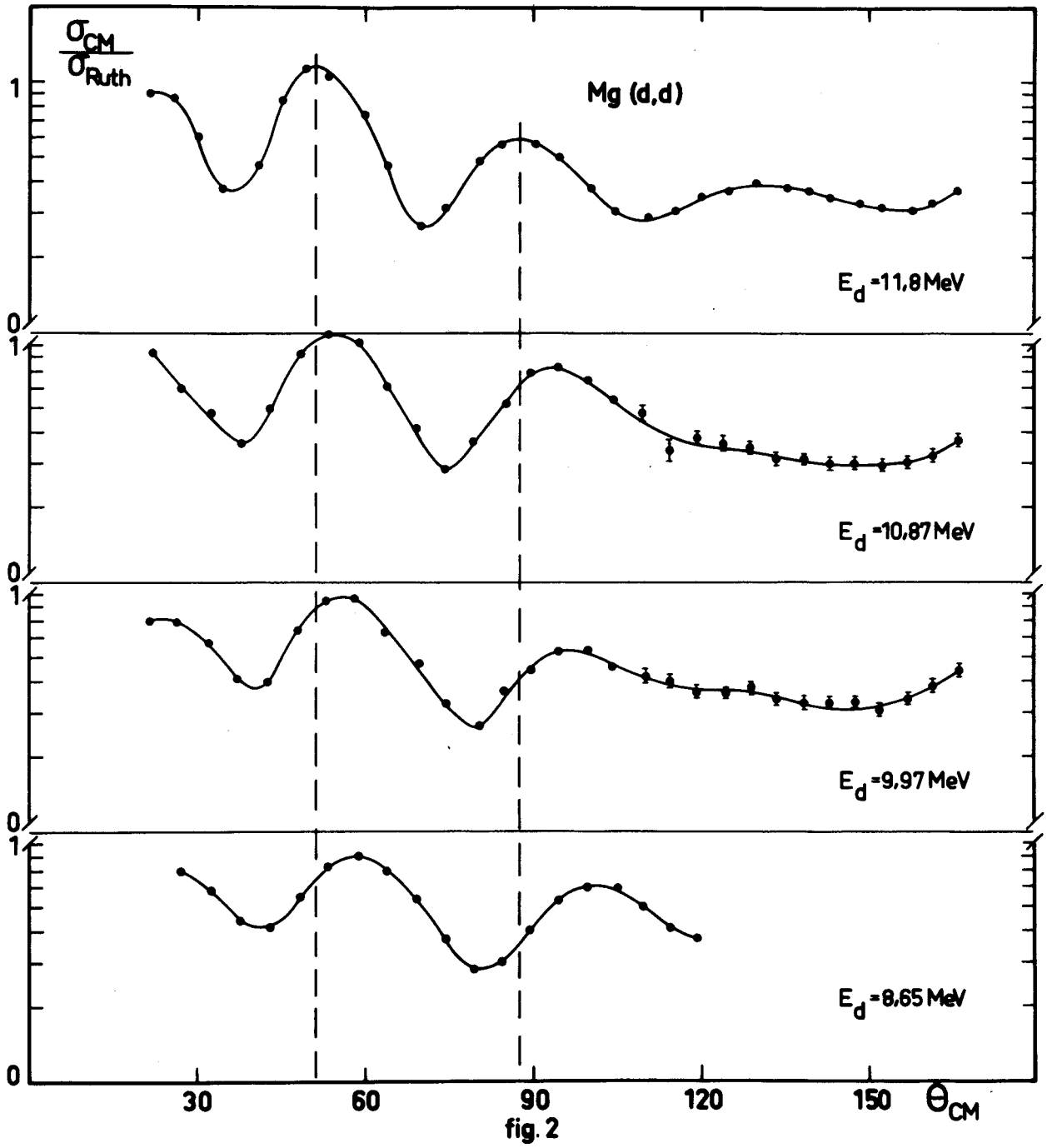
σCM / σRuth
Mg (d,d)
Ed =11,8 MeV
Ed =10,87 MeV
Ed =9,97 MeV
Ed =8,65 MeV
1
0
30
60
90
120
150
θCM

fig. 2

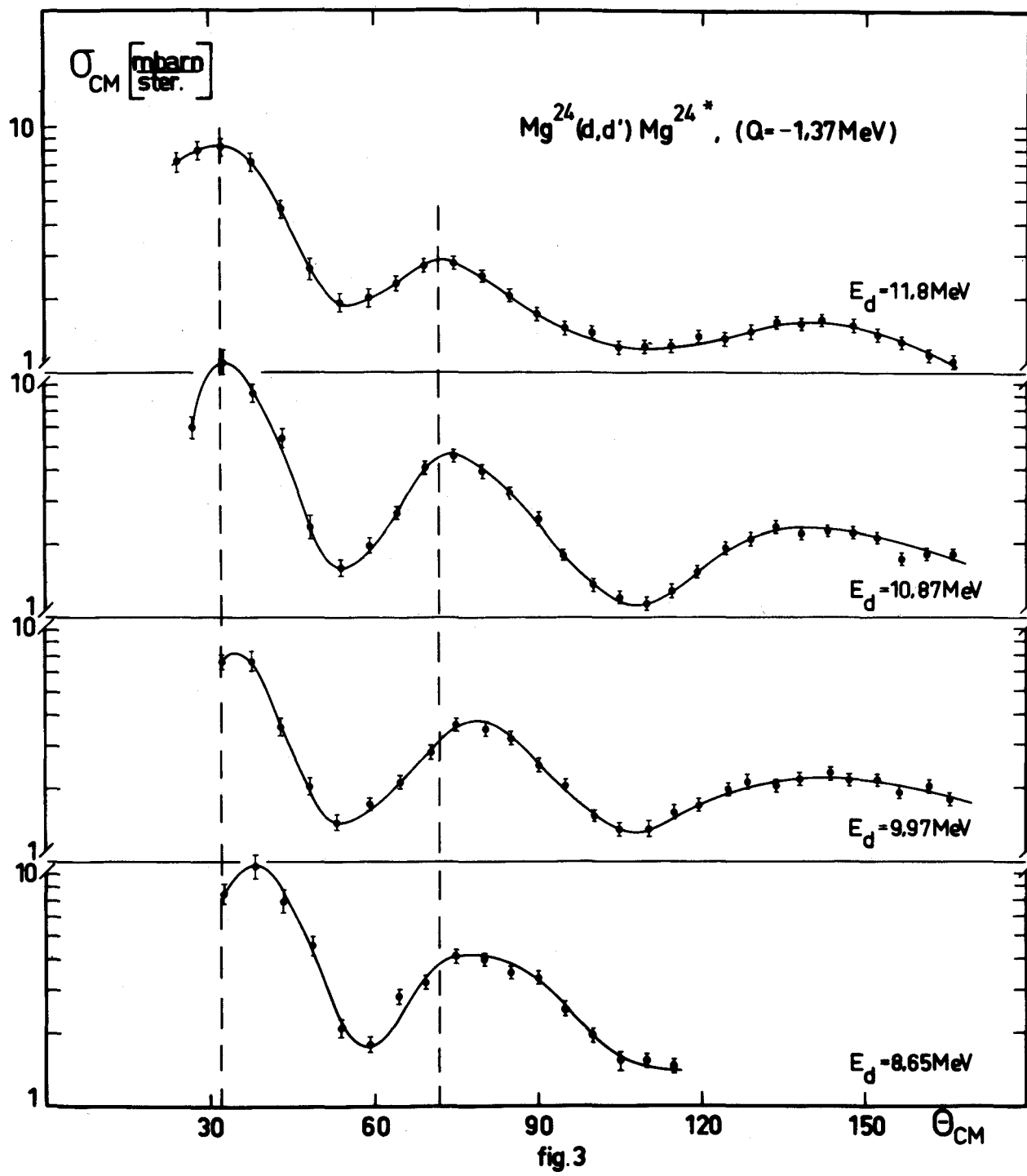
σCM [mbarn ster.]
Mg24(d,d') Mg24*, (Q=-1,37MeV)
Ed=11,8MeV
Ed=10,87MeV
Ed=9,97MeV
Ed=8,65MeV
10
1
30
60
90
120
150
ΘCM

fig.3

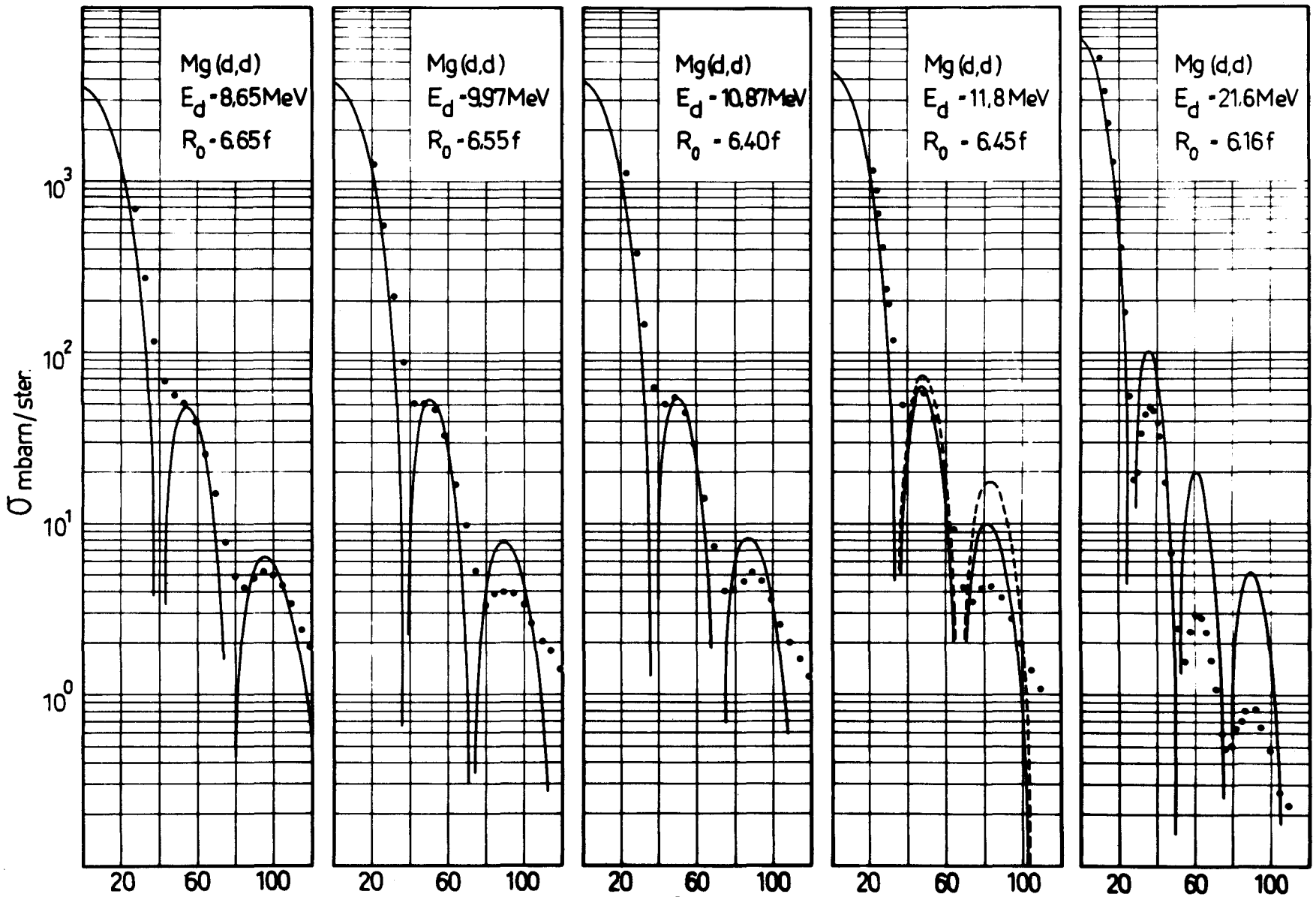
Mg (d,d)
E_d - 8,65MeV
R_0 - 6.65f
Mg (d,d)
E_d - 9.97MeV
R_0 - 6.55f
Mg(d,d)
E_d - 10,87MeV
R_0 - 6.40f
Mg (d,d)
E_d - 11,8 MeV
R_0 - 6.45f
Mg (d,d)
E_d - 21.6MeV
R_0 - 6.16f
10^3
10^2
10^1
10^0
σ mbarn/ster.
20
60
100
θ_{cm}

fig. 4

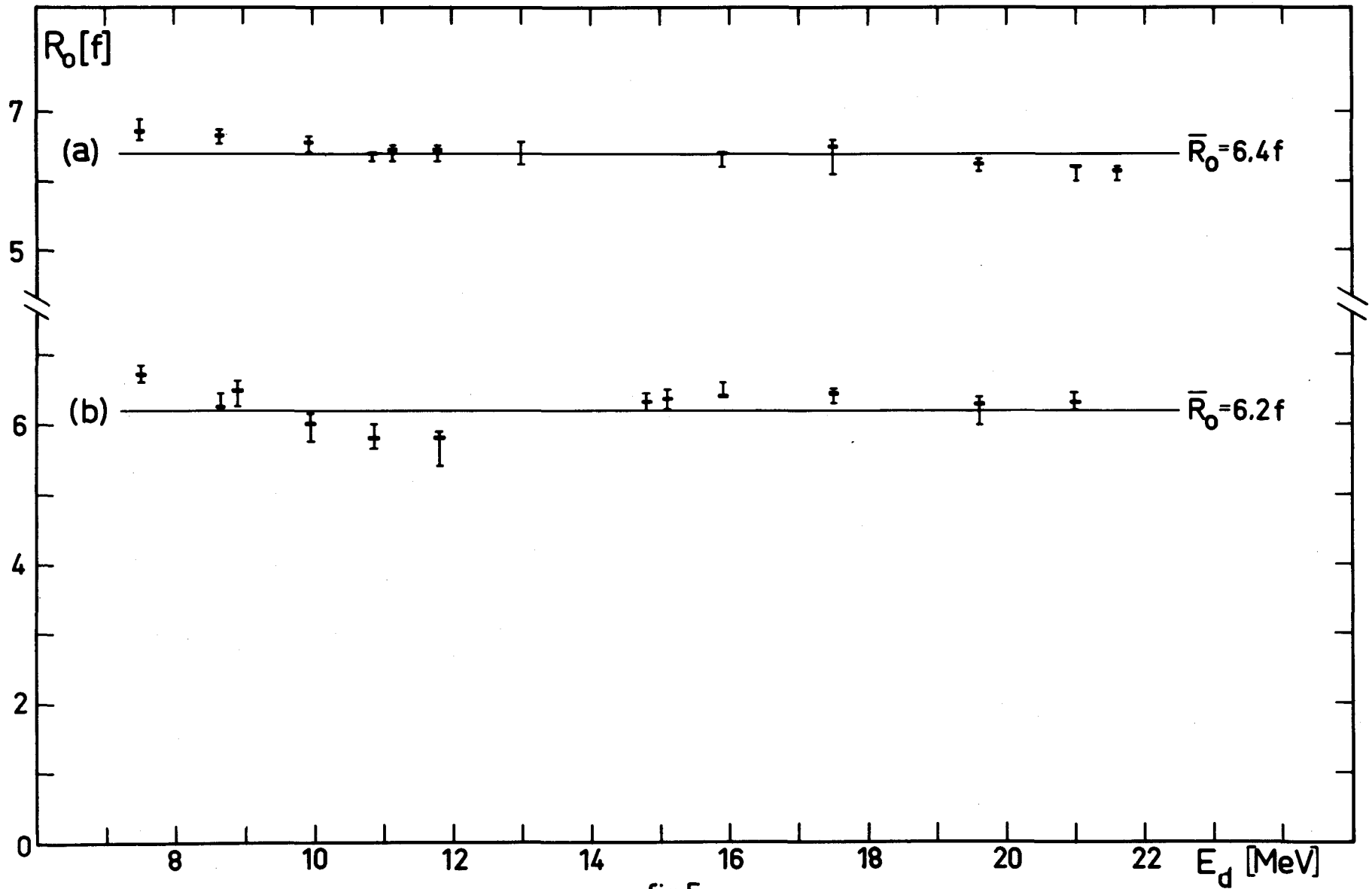

fig.5

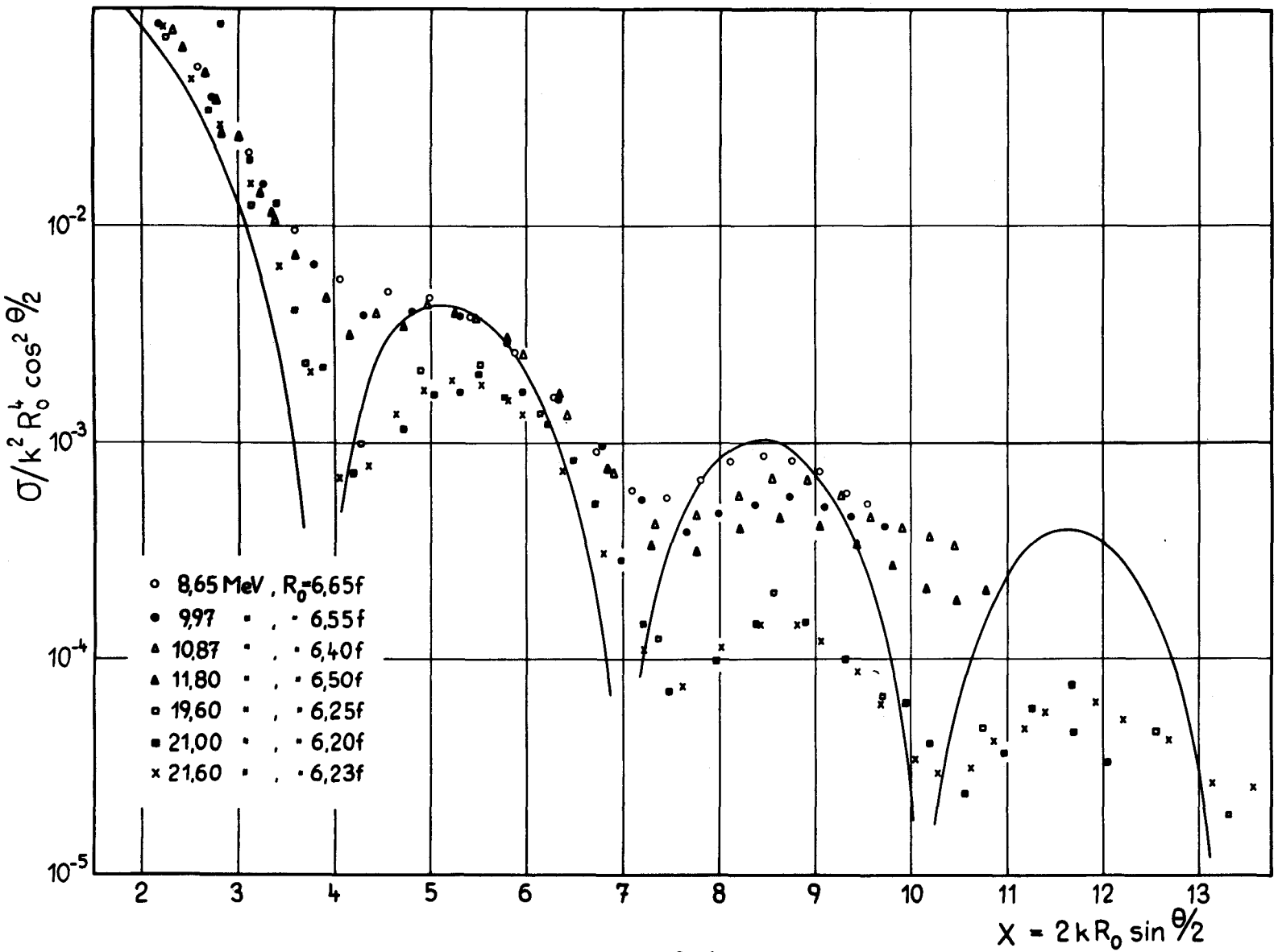
10^{-2}
10^{-3}
10^{-4}
10^{-5}
$\sigma/k^2 R_0^4 \cos^2 \theta/2$
2
3
4
5
6
7
8
9
10
11
12
13
$X = 2kR_0 \sin \theta/2$
8,65 MeV , R_0=6,65f
9,97 " , " 6,55f
10,87 " , " 6,40f
11,80 " , " 6,50f
19,60 " , " 6,25f
21,00 " , " 6,20f
21,60 " , " 6,23f

fig.6

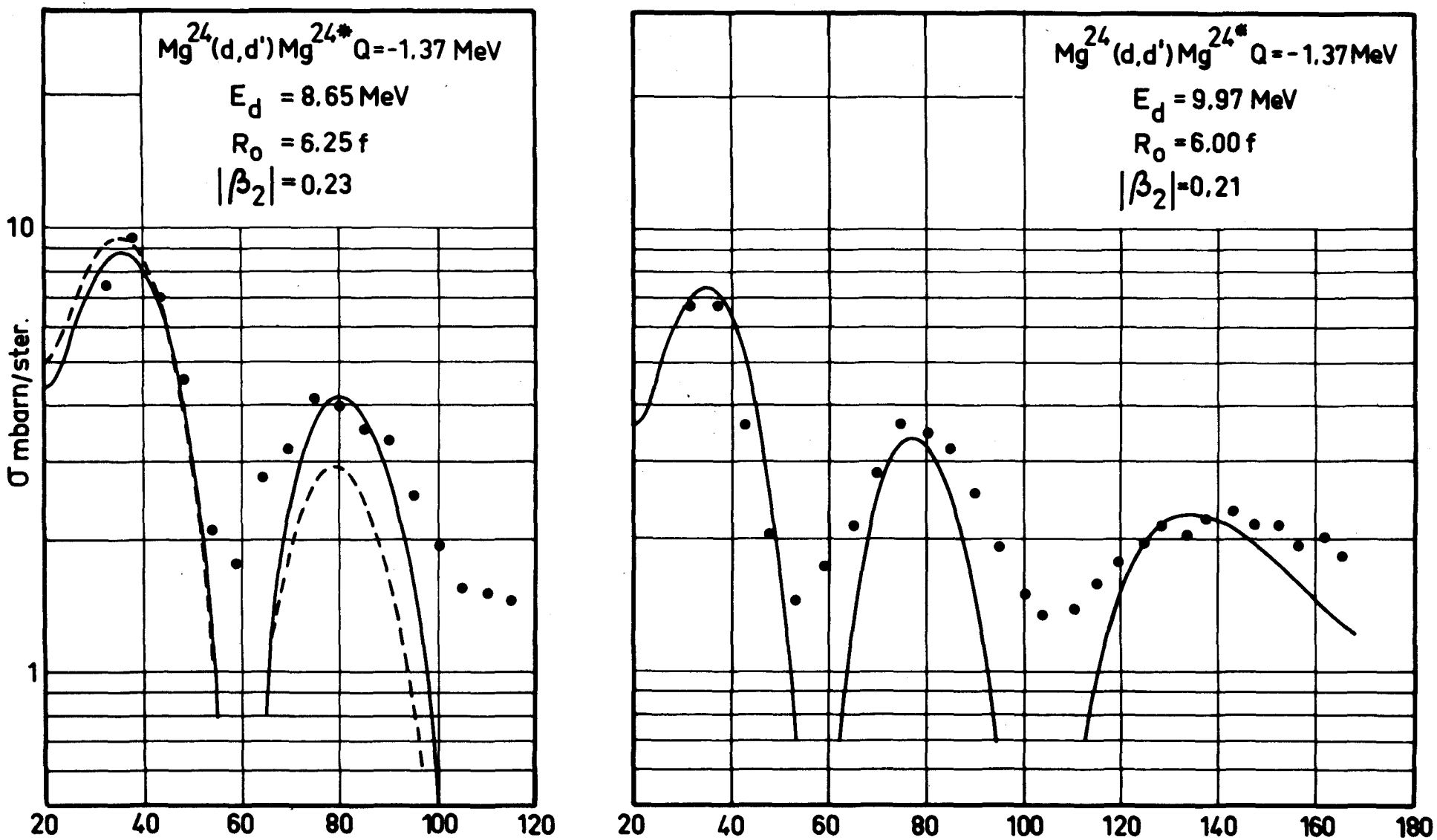
$Mg^{24}(d,d')Mg^{24*}$ Q=-1.37 MeV
E_d = 8.65 MeV
R_o = 6.25 f
$|\beta_2|$ = 0.23
$Mg^{24}(d,d')Mg^{24*}$ Q=-1.37 MeV
E_d = 9.97 MeV
R_o = 6.00 f
$|\beta_2|$ = 0.21
σ mbarn/ster.
10
1
20
40
60
80
100
120
140
160
180
θ_{CM}

fig. 7a+b

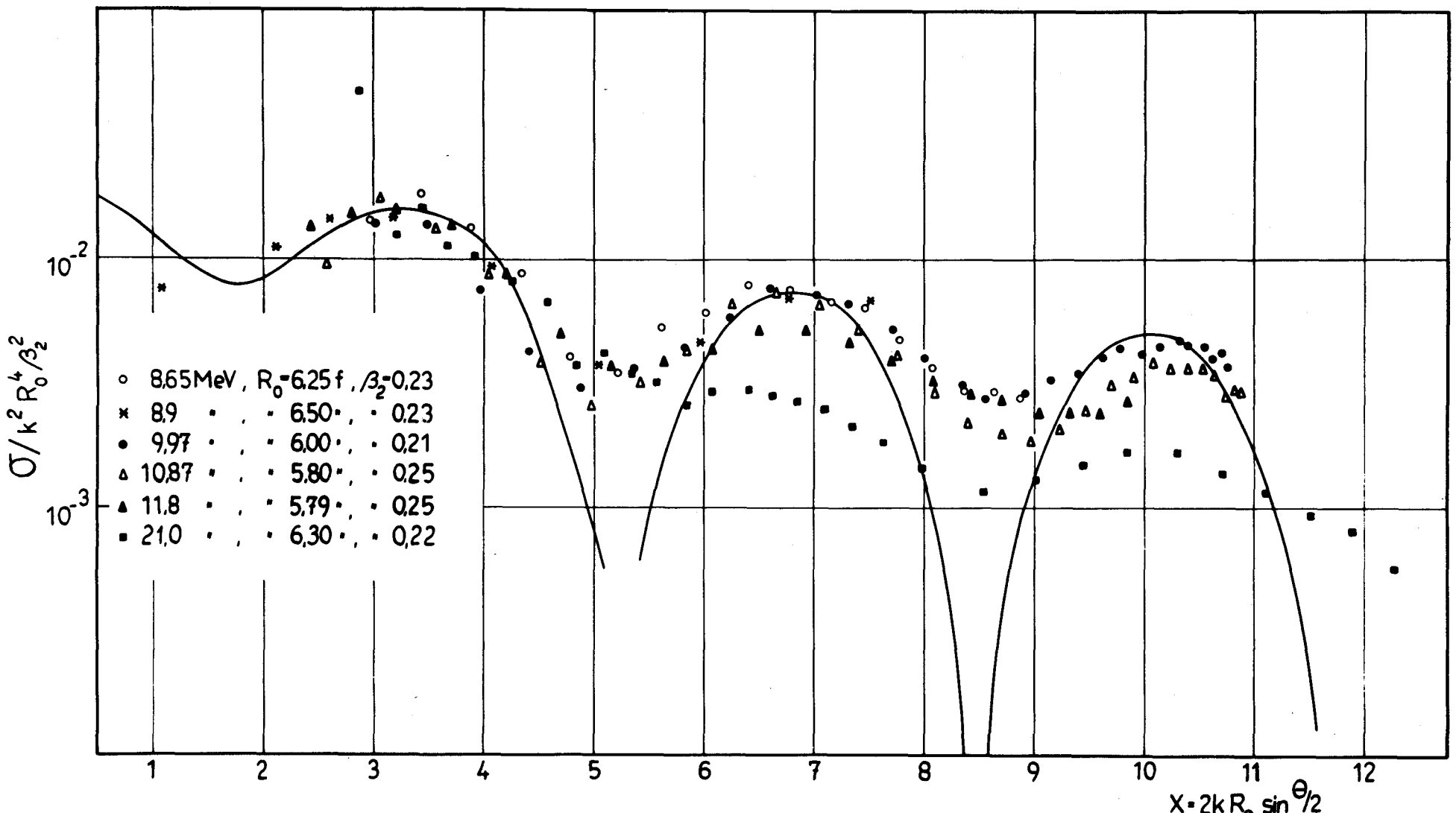
10^{-2}
10^{-3}
$\sigma/k^2 R_0^4 \beta_2^2$
○ 8.65 MeV , R_0=6.25 f , β_2=0.23
× 8.9 " , " 6.50 " , " 0.23
● 9.97 " , " 6.00 " , " 0.21
△ 10.87 " , " 5.80 " , " 0.25
▲ 11.8 " , " 5.79 " , " 0.25
■ 21.0 " , " 6.30 " , " 0.22
1
2
3
4
5
6
7
8
9
10
11
12
$X = 2k R_0 \sin \theta/2$

fig. 8